Thermal Impedance Measurement of Thick-Film Resistor in High-Frequency Range Using Single-Detector IR System

Maria Strąkowska, Bogusław Więcek
Lodz University of Technology, Institute of Electronics, Poland

Gilbert De Mey
University of Ghent, Department of Electronics and Information Systems, Belgium

Abstract: This paper presents an innovative and simple method of high-frequency thermal impedance measurement using infrared (IR) technique. The method is based on the Fourier transformation of the input power signal and the thermal response of the object after supplying the heat source with square-wave current of different frequencies. The experiment was carried out using a single-detector, low-cost infrared system equipped with a photovoltaic detector module to measure the thermal impedance of an SMD thick-film resistor. Both the simulation using a compact thermal model and the measurement results are discussed.

Keywords: IR thermography, thermal impedance, Fourier transform, thermography measurements

1. Introduction

The thermal characteristics of an object in a dynamic state is of interest to many fields, e.g. electronics and electrical engineering [1–4], automation and control [5–12] and others. In many cases, the measurement of thermal impedance over a large frequency range is a problem. Most often, thermal impedance estimation is done by inverse modelling of the object or other indirect methods, including advance image and signal processing. Several notable methods can be distinguished, such as network identification by deconvolution (NID) [1–3], a computer-aided program for analysing time series and identifying disturbed systems (CAPTAIN) [20, 13], transfer function estimation (TFEST) [14] or the Vector Fitting algorithm to solve the inverse problem of heat exchange [13, 15, 4]. There are also commercial systems available for measuring the thermal impedance of objects [16]. High resolution IR cameras with a high frame-rate of at least 1000 FPS are required to measure high-frequency thermal impedance. In addition, special equipment must be used to synchronize temperature and power. Such a device is mainly used in electronics for thermal characterization of packaged semiconductor devices (diodes, BJTs, power MOSFETs, IGBTs, power LEDs) and multi-die power devices.

This paper presents one of the first experimental attempts to estimate thermal impedance by non-contact temperature measurement using a low-cost IR system. The presented approach allows obtaining results for a wide frequency range up to hundreds of Hz.

In order to confirm the correctness of proposed measurement procedure of thermal impedance, simple RC thermal model was developed. It is based on the thermo-electrical analogy which is well known for estimation the thermal parameters since 1936 [16–19].

2. Thermal compact model of the thick-film resistor

A simple thermal model was developed for a surface mounted resistor in the 1206 package. The cross-section of its structure is shown in Fig. 1.

It consists of a layered structure with a thick resistive layer deposited on an alumina substrate by screen printing. The resi-

Autor korespondujący:
Maria Strąkowska, maria.strakowska@p.lodz.pl

Artykuł recenzowany
nadesłany 16.09.2023 r., przyjęty do druku 09.01.2024 r.

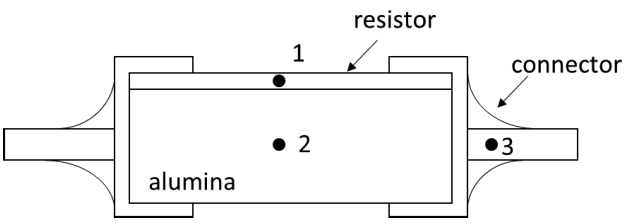

Fig. 1. Cross section of the resistor with marked nodes
Rys. 1. Przekrój rezystora z zaznaczonymi węzłami

stance value depends on the shape of the resistive layer, which does not cover the entire alumina substrate. Electrodes and connecting wires that play an important role in heat dissipation were included in the modelling.

A simple compact thermal model of such a resistor consisting of a network of thermal resistances R_{th} and heat capacities C_{th} is shown in Fig. 2. The resistor is stimulated by an electrical power supplied to the heat source located on top of its structure. The power is then transferred to the ambient via free convection, modeled with R_{1a} at the top. At the bottom, heat is transferred through the alumina substrate and then to the ambient via convection represented by resistor R_{2a}. Resistor R_{3a} is responsible for cooling by convection through connecting wires. Due to the axial symmetry, only half of the resistor is modelled.

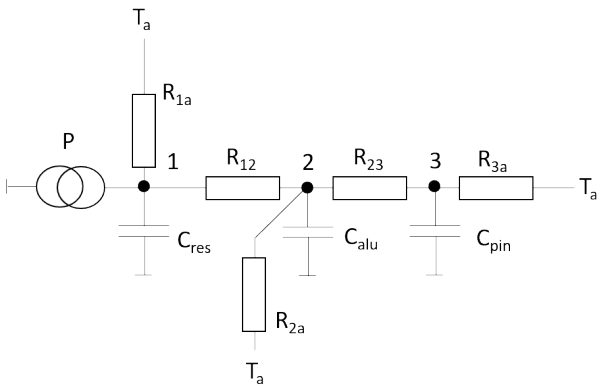

Fig. 2. $R_{th}C_{th}$ network of the compact thermal model of a thick-film resistor
Rys. 2. Sieć $R_{th}C_{th}$ kompaktowego modelu termicznego rezystora grubowarstwowego

The dissipated power P in the resistive layer (node 1) is transferred by conduction down to the alumina substrate (node 2) and then horizontally to the electrodes (node 3). The thermal resistances are named R_{12} and R_{23}. They correspond to the half the thickness of the resistor and an alumina layer in the vertical and horizontal directions as it is shown by (2) and (3). In addition, power is transferred to the ambient through electrical connectors soldered to the pins of the resistor. Material parameters, their descriptions and dimensions are in table 1.

The compact $R_{th}C_{th}$ model of the resistor consists of three nodes. In result, the mathematical form of the model is represented by the set of three linear equations (1) that can be solved analytically using the node potential method.

$$\left.\begin{aligned} \frac{T_1 - T_2}{R_{12}} + T_1 j\omega C_{res} + \frac{T_1 - T_a}{R_{1a}} &= P \\ \frac{T_1 - T_2}{R_{12}} = \frac{T_2 - T_3}{R_{23}} + T_2 j\omega C_{alu} + \frac{T_2 - T_a}{R_{2a}} &\\ \frac{T_2 - T_3}{R_{23}} = T_3 j\omega C_{pin} + \frac{T_3 - T_a}{R_{3a}} & \end{aligned}\right\} \quad (1)$$

Resistor R_{12} is associated to the surface $S_{av} = S_{rv}$ where the heat flows vertically. Similarly, resistor R_{23} correspond to the horizontal heat flow through the surface S_{ah}, as shown in (2).

Table 1. Parameters of the compact model of the resistor
Tabela 1. Parametry kompaktowego modelu rezystora grubowarstwowego

Parameter	Value	Unit	Description
k_r	10	W/(m · K)	Thermal conductivity of the resistive layer
k_a	15	W/(m · K)	Thermal conductivity of the alumina layer
k	300	W/(m · K)	Thermal conductivity of the wire
k_{pin}	20	W/(m · K)	Thermal conductivity of the soldered pin
l_r, l_a	10^{-3}	m	Length of the resistive and alumina part
l_{pin}	$2{\cdot}10^{-3}$	m	Length of the soldered connector and the wire
w_r, w_a	10^{-3}	m	Width of the resistive and alumina part
h_r	$5{\cdot}10^{-5}$	m	Height of the resistive part
h_a	$4.4{\cdot}10^{-4}$	m	Height of the alumina part
S_{pin}	10^{-6}	m^2	Surface of the soldered connector and wire
h_{up}	20	W/(m^{2}K)	Heat transfer coefficient for the top surface
h_{bot}	15	W/(m^{2}K)	Heat transfer coefficient for the bottom surface
h_{wire}	30	W/(m^{2}K)	Heat transfer coefficient for wire
c_{vth_res}	$2{\cdot}10^6$	J/(m^{3}K)	Volumetric thermal capacity of resistor
c_{vth_alu}	$1.9{\cdot}10^6$	J/(m^{3}K)	Volumetric thermal capacity of alumina
c_{vth_pin}	$2{\cdot}10^6$	J/(m^{3}K)	Volumetric thermal capacity of the pins

$$\left.\begin{aligned} R_{12} &= \frac{h_r}{2 \cdot k_r S_{rv}} + \frac{h_a}{2 \cdot k_a S_{av}} \\ R_{23} &= \frac{w_a}{2 \cdot k_a S_{av}} + \frac{l_{pin}}{k_{pin} S_{av}} \end{aligned}\right\} \quad (2)$$

The convection cooling is applied to the top and bottom sides of the resistor. Resistor R_{1a} describes convective cooling on the top while R_{2a} on the bottom side (3).

$$\left.\begin{aligned} R_{1a} &= \frac{h_r}{2 \cdot k_r S_{rv}} + \frac{1}{h_{up} S_{rv}} \\ R_{2a} &= \frac{h_a}{2 \cdot k_a S_{av}} + \frac{1}{h_{bot} S_{av}} \end{aligned}\right\} \quad (3)$$

Resistor R_{3a} is associated to the convective cooling of the wire that transfer heat to the environment. The value of R_{3a} resistance is derived assuming the infinite length of the external connection and takes a form (4).

$$R_{3a} = \frac{1}{\pi r \sqrt{2 h_{wire} k_r}} \quad (4)$$

where r, k are radius and thermal conductivity of a wire, respectively and h_{wire} denotes the convective heat transfer coefficient for the wire.

The thermal capacitances related to the resistive layer, alumina, and soldered part can be expressed by (5).

$$\left.\begin{aligned} C_{res} &= c_{vth\_res} \cdot V_{res} \\ C_{alu} &= c_{vth\_alu} \cdot V_{alu} \\ C_{pin} &= c_{vth\_pin} \cdot V_{pin} \end{aligned}\right\} \quad (5)$$

where c_{vth_res}, c_{vth_alu}, c_{vth_pin} corresponding to the volumetric thermal capacitances and V_{res}, V_{alu}, V_{pin} denote the volumes of the resistive layer, alumina substrate and the pin parts of the modelled resistor, respectively.

The values of model parameters, like surface areas, length, volumes, thermal conductivities and capacitance of the material were determined through experimental means due to the fact that the exact dimensions are not available in the literature. Heat is conducted along the resistive layer; thus the assumed length is also smaller than the dimension of the entire resistor. Furthermore, the cooper connector is assumed to be not only the metal pad but also the solder and the wire so its parameters are also estimated. Such assumptions and obtained values are not so important due to the fact that the resistor is just the example to present the method of the thermal impedance measurement in high-frequency and confirmed that it agrees with the thermal modelling results of the measured object.

The resistances and capacitances obtained using above values of parameters are listed in table 2.

During the fundamental research, it is always recommended to simulate the heat transfer in a sample prior in order to predict the results of experiments. The graph in Fig. 3 presents the plot of thermal impedance $Z_{th}(j\omega)$ – Nyquist plot. Each of the half circles corresponds to each of the node of the $R_{th}C_{th}$ network of the proposed compact model that correspond to resistive, alumina and solder layers in the physical device.

For the high frequency range, the Nyquist plot follows the –45° line crossing it at two points for the frequencies 41.38 Hz and 6.02 Hz, as shown in Fig. 4.

Table 2. Estimated values of thermal resistances and capacitances of compact thermal model RthCth of the thick-film resistor
Tabela 2. Wyznaczone wartości rezystancji I pojemności termicznych kompaktowego modelu RthCth rezystora grubowarstwowego

Parameter	Value	Unit
R_{12}	31.83	K/W
R_{23}	133.33	
R_{1a}	$1.0 \cdot 10^5$	
R_{2a}	$1.3 \cdot 10^5$	
R_{3a}	212.21	
C_{res}	$1.0 \cdot 10^{-4}$	J/K
C_{alu}	$8.38 \cdot 10^{-4}$	
C_{pin}	0.04	

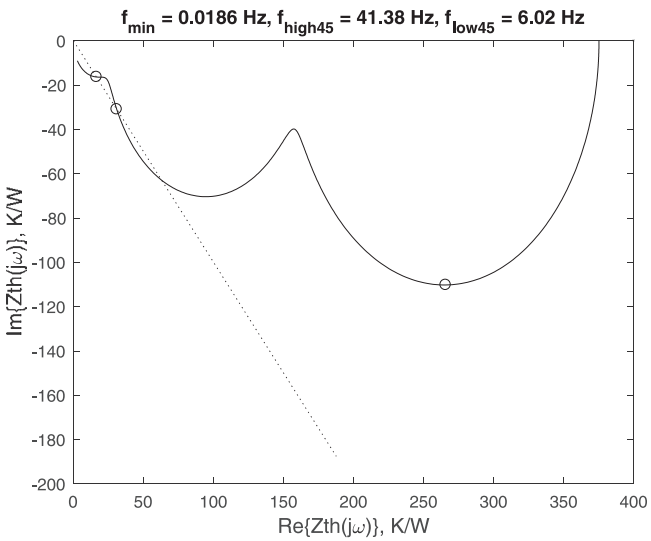

Fig. 3. Simulated thermal impedance Zth(jω) for compact heat transfer model of the SMD1206 resistor
Rys. 3. Wykres impedancji termicznej Zth(jω) dla kompaktowego modelu przepływu ciepła w rezystorze SMD1206 uzyskany za pomocą symulacji

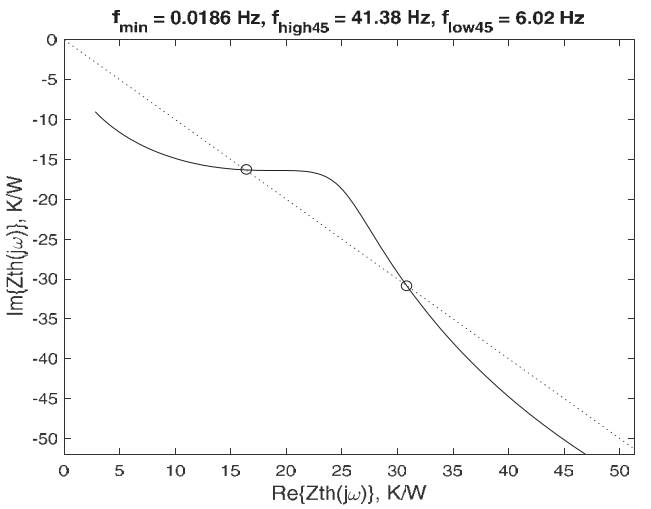

Fig. 4. Zoomed part of the Nyquist plot for high range of the frequencies showing the crossing points with –45° line
Rys. 4. Wykres Nyquista powiększony w zakresie dużych częstotliwości przedstawiający przecięcie z linią nachyloną pod kątem –45°

3. Measurement methodology and experimental results

The measured object is thermally excited with electrical current of the appropriate frequency by switching the current on and off. Both current and power take the form of a square wave signal as shown in Fig. 5a. The thermal response to such excitation is measured using a single-detector infrared head as shown in Fig. 5b. The frequency of the input signal changes to characterize the object in the selected frequency range. In order to limit analysis errors, a single period is taken into account for further processing – Fig. 5c and Fig. 5d. The Fourier transform is applied to both the input and output signal to calculated the fundamental harmonics for estimation the thermal impedance.

It is also possible to consider more harmonics to estimate the thermal impedance for a higher frequency range, but it can generate unexpected errors because these signals are quite small.

Having the first harmonics one can estimate the real and imaginary part of the thermal impedance and directly plot the Nyquist plot for the measured object.

$$Z_{th}(j\omega) = \frac{T(j\omega)}{P(jw)} = \left|Z_{th}(j\omega)\right| e^{j\varphi} \tag{6}$$

where $T(j\omega)$ is the value of fundamental harmonic of the output signal (thermal response), and $P(j\omega)$ is the fundamental harmonic of the input power signal.

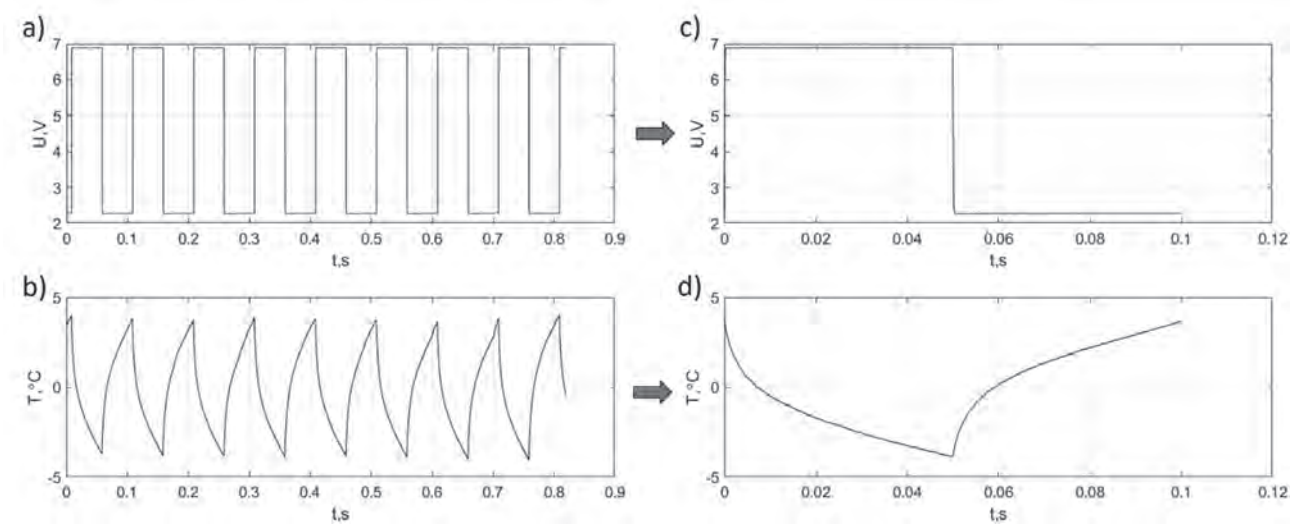

Fig. 5. 10 Hz input power signal (a) and measurement result for such excitation (b). 0ne cut period for input signal (c) and for the output (d)
Rys. 5. Sygnał wejściowy o częstotliwości 10 Hz (a) oraz wynik pomiaru dla takiego pobudzenia (b). Jeden okres sygnału wejściowego (c) oraz wyjściowego (d)

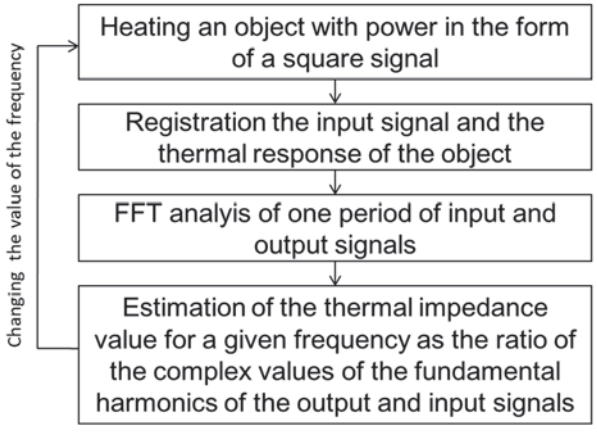

Fig. 6. Following steps in measurement procedure
Rys. 6. Następujące po sobie kroki w procedurze pomiaru

The scheme of the following steps in measurement procedure shows Figure 6.

Measurement stand consist of programmable frequency signal generator that sends the signal for conditioning by the power driver to heat up the thick-film resistor. Power outputs were connected by the thin wires to the resistor. The IR head with the single photovoltaic detector generates the temperature signal varying in time synchronously with the power excitation, as presented in Fig. 7. Finally, the Fourier transform is used to calculate the fundamental harmonics of both signals.

The measured resistor was heated by the power obtained from the voltage signal of around 7 V amplitude and current limit at 150 mA. The frequency was changing by a microcontroller connected to power driver made of MOS transistors. Frequency generator is used for changing the power signal frequency in the range 2–100 Hz. Analog-to-digital conversion was done with the sampling frequency $f_s = 10$ kHz. The 27 Ω resistor in

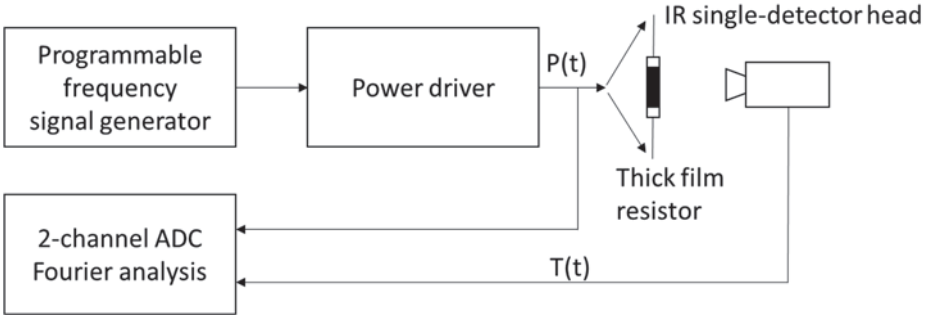

Fig. 7. Scheme of the measurement setup
Rys. 7. Schemat stanowiska pomiarowego

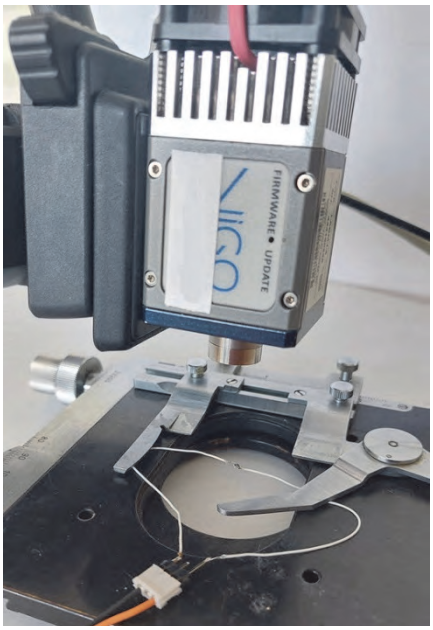

Fig. 8. Photo of Vigo camera and measured resistor
Rys. 8. Zdjęcie modułu termowizyjnego Vigo i badanego rezystora

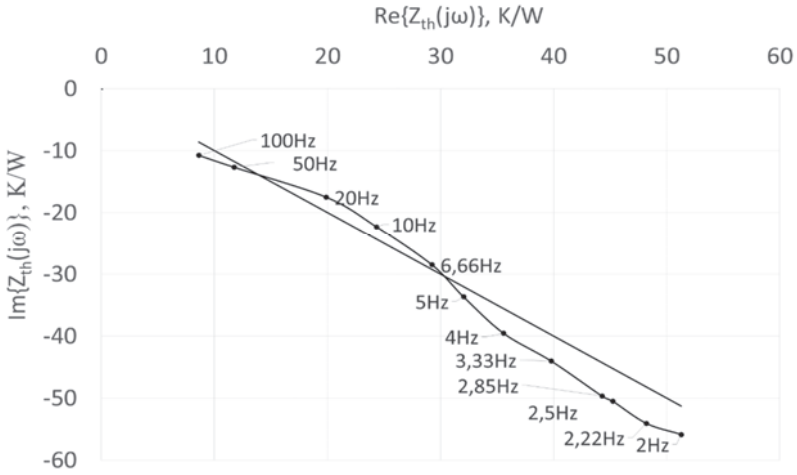

Fig. 9. Nyquist plot of thermal impedance obtained from the measurement
Rys. 9. Wykres Nyquista impedancji termicznej uzyskany z pomiaru

1206 case was the measured object. The measurement setup with single photovoltaic sensor registering oscillating power and temperature is presented in Fig. 8.

The part of the Nyquist plot of thermal impedance measured in the high frequency range is presented in Fig. 9.

The obtained shape of the Nyquist plot for the high frequency range (Fig. 9) is similar to that obtained from the simulation (Fig. 4). The thermal impedance curve crosses the –45° line for frequencies around 41 Hz and 6 Hz. This confirmed that the proposed thermal model corresponds to the measured thermal object. Finally, it can be concluded that using this method, the correct thermal impedance can be measured simply and reliably.

4. Conclusions

The article presents a simple method of measuring thermal impedance for the high frequency range. It consists in supplying the tested device with rectangular excitation of variable frequency and calculating the first harmonics of power and temperature. Temperature measurement is carried out in a non-contact way, using an inexpensive, single-detector IR system. The main result of the measurement – the Nyquist plot of thermal impedance in the frequency range 2–100 Hz, agrees with the modeling results.

The presented results confirmed that both the model and the measurement generate convergent results. The proposed method of measuring thermal impedance is fast, reliable, non-invasive and non-contact. It can also be used in biomedical applications, e.g. for screening and diagnosis of skin tissue diseases. This method simplifies the identification of thermal objects in dynamic states and can be an alternative to the use of expensive, cooled laboratory thermal imaging cameras.

References

1. Szekely V., *On the representation of infinite-length distributed RC one-ports.* "IEEE Transactions on Circuits and Systems", Vol. 38, No. 7, 1991, 711–719, DOI: 10.1109/31.135743.
2. Szekely V., *Identification of RC networks by deconvolution: Chances and limits.* "IEEE Transactions on Circuits and Systems", Vol. 45, No. 3, 1998, 244–258, DOI: 10.1109/81.662698.
3. Vermeersch B., *Thermal AC Modelling, Simulation and Experimental Analysis of Microelectronic Structures Including Nanoscale and High-Speed Effects.* PhD Thesis, Gent University, Gent, Belgium, 2009.
4. Gustavsen B., *Improving the pole relocating properties of vector fitting.* "IEEE Transactions on Power Delivery", Vol. 21, No. 3, 2006, 1587–1592, DOI: 10.1109/TPWRD.2005.860281.
5. Garnier H., Mensler M., Richard A.A., *Continuous-time Model Identification from Sampled Data: Implementation Issues and Performance Evaluation.* "International Journal of Control", Vol. 76, No. 13, 2003, 1337–1357, DOI: 10.1080/0020717031000149636.
6. Marco S., Palacin J., Samitier J., *Improved multiexponential transient spectroscopy by iterative deconvolution.* "IEEE Transactions on Instrumentation and Measurement", Vol. 50, No. 3, 2001, 774–780, DOI: 10.1109/19.930453.
7. Ljung L., *Experiments with Identification of Continuous-Time Models.* "IFAC Proceedings Volumes", Vol. 42, No. 10, 2009, 1175–1180, DOI: 10.3182/20090706-3-FR-2004.00195.
8. Yarman B.S., Kilinc A., Aksen A., *Immitance Data Modelling via Linear Interpolation Techniques: A Classical Circuit Theory Approach.* "International Journal of Circuit Theory and Applications", Vol. 32, No. 6, 2004, 1467–1563, DOI: 10.1002/cta.295.
9. Jibia A.U., Salami M.J., *An Appraisal of Gardner Transform-Based Method of Transient Multiexponential Signal Analysis.* "International Journal of Computer Theory and Engineering", Vol. 4, No. 1, 2012, 16–24, DOI: 10.7763/IJCTE.2012.V4.420.
10. De Tommasi L., Magnani A., De Magistris M., *Advancements in the identification of passive RC networks for compact modeling of thermal effects in electronic devices and systems.* "International Journal of Numerical Modelling", Vol. 31, No. 3, 2017, 64–66, DOI: 10.1002/jnm.2296.
11. Shindo Y., Noro O., *Effective frequency range of ladder network realization for complex permeability of magnetic sheets.*

"IEEJ Transactions on Electrical and Electronic Engineering", Vol. 9, No. 51, 2014, 64–66, DOI: 10.1002/tee.22035.
12. Wang K., Chen M.Z.Q., Chen G., *Realization of a transfer function as a passive two-port RC ladder network with a specified gain.* "International Journal of Circuit Theory and Applications", Vol. 45, No. 11, 2017, 1467–1481, DOI: 10.1002/cta.2328.
13. Karimifard P., Gharehpetian G.B., Tenbohlen S., *Localization of winding radial deformation and determination of deformation extent using vector fitting-based estimated transfer function.* "European Transactions on Electrical Power", Vol. 19, No. 5, 2013, 749–762, DOI: 10.1002/etep.253.
14. Strakowska M., Chatzipanagiotou P., De Mey G., Chatziathanasiou V., Więcek B., *Novel software for medical and technical Thermal Object Identification* (*TOI*) *using dynamic temperature measurements by fast IR cameras,* Proceedings of QIRT 2018, Berlin, 531–538, http://qirt.gel.ulaval.ca/dynamique/index.php?idD=78.
15. Strąkowska M., Chatzipanagiotou P., De Mey G., Więcek B., *Multilayer thermal object identification in frequency domain using IR thermography and vector fitting.* "International Journal of Circuit Theory and Applications", Vol. 48, No. 9, 2020, 1523–1533, DOI: 10.1002/cta.2845.
16. Beuken C.L. *Wärmeverluste bei periodisch betriebenen elektrischen* Öfen*: eine neue Methode zur Vorausbestimmung nicht-stationärer Wärmeströmungen.* PhD Thesis, Bergakadem Freiberg, Triltsch & Huther, 1936.
17. Minkina W., Chudzik S., *Pomiary parametrów cieplnych materiałów termoizolacyjnych – przyrządy i metody.* Wydawnictwo Politechniki Częstochowskiej, Częstochowa 2004, ISBN 83-7193-216-2.
18. Minkina W., *On some singularities in space discretization while solving the problems of unsteady heat conduction.* "Experimental Technique of Physics", Vol. 41, No. 1, 1995, 37–54.
19. Minkina W., *Space discretization in solving chosen problems of unsteady heat conduction by means of electric modelling.* "Elektrotechnickỳ časopis", Vol. 45, No. 1, 1994, 8–15.

Other sources

20. CAPTAIN-Computer-Aided Program for Time Series Analysis and Identification of Noisy Systems, www.es.lancs.ac.uk/cres/captain/ (accessed on 20.08.2023).
21. T3ster, https://plm.sw.siemens.com/en-US/simcenter/physical-testing/t3ster/ (accessed on 20.08.2023).

Pomiar impedancji termicznej rezystora grubowarstwowego w zakresie dużych częstotliwości przy zastosowaniu systemu termowizyjnego z pojedynczym detektorem

Streszczenie: Artykuł przedstawia nową, prostą metodę pomiaru impedancji termicznej w zakresie dużych częstotliwości przy wykorzystaniu technik podczerwieni. W tym celu zastosowano transformację Fouriera sygnału wejściowego oraz odpowiedzi termicznej badanego obiektu po pobudzeniu go źródłem ciepła w postaci prądu o kształcie prostokątnym i o różnej częstotliwości. Eksperyment został przeprowadzony przy użyciu taniego systemu termowizyjnego z pojedynczym fotowoltaicznym detektorem podczerwieni w celu pomiaru impedancji termicznej grubowarstwowego rezystora SMD. Badana próbka pobudzana była sygnałem prostokątnym o różnych częstotliwościach z zakresu 2–100 Hz, a system IR rejestrował zmianę wartości jego temperatury. W celu potwierdzenia poprawności uzyskanych wyników badań opracowano model kompaktowy RthCth struktury rezystora oraz podłączonych do niego wyprowadzeń. Przeprowadzone symulacje potwierdziły poprawność zarówno metody pomiaru jak i opracowanego modelu termicznego. Kształt wykresów Nyquista impedancji termicznej dla modelu jak i pomiaru jest zbliżony. W zakresie dużych częstotliwości oba wykresy zbliżają się do linii o nachyleniu –45° przekraczając tę linię w dwóch punktach. Zaproponowana metoda pomiaru impedancji termicznej jest szybka, niezawodna, nieinwazyjna i bezkontaktowa. Może być wykorzystana również do zastosowań biomedycznych np. do diagnostyki chorób skóry. Metoda ta upraszcza identyfikację termiczną obiektów w stanie dynamicznym i może być alternatywą dla stosowania do tego celu drogich systemów termowizyjnych z detektorami chłodzonymi.

Słowa kluczowe: termografia w podczerwieni, impedancja cieplna, przekształcenie Fouriera, pomiary termograficzne

Maria Strąkowska, PhD, Eng

maria.strakowska@p.lodz.pl
ORCID: 0000-0001-6246-0086

She received her PhD degree in electronic in 2017 at the Lodz University of Technology (LUT). Since 2017, she has been an employee of the Institute of Electronics of the Lodz University of Technology as an assistant professor. Her scientific interests focus on computer modeling of heat transfer phenomena in biomedicine and electronics. In addition, she conducts research in the field of thermal image processing and infra-red imaging system measurements.

Prof. Gilbert De Mey, PhD

Gilbert.DeMey@UGent.be
ORCID: 0000-0001-6083-8380

He is a full professor at Ghent University. He conducts research on thermal problems in electronic systems and related fields such as textile engineering. His main area of research concerns the issues of heat transfer modelling, thermographic measurements and applications. He is a co-author of hundreds of papers on heat transfer in electronic components and systems, including studies of convection and radiation.

Prof. Bogusław Więcek, DSc, PhD, Eng

boguslaw.wiecek@p.lodz.pl
ORCID: 0000-0002-5003-1687

He is the head of the Department of Electronic Circuits and Thermography at the Institute of Electronics of the Lodz University of Technology. His research interests include: industrial and biomedical applications of IR thermography, heat transfer modeling and the development of advanced analog and digital IR systems. He is responsible for organizing the largest conference on thermography in Central and Eastern Europe every two years, entitled Thermography and Infrared Thermometry.